

ESTIMATING TIME-VARYING NETWORKS

BY MLADEN KOLAR, LE SONG, AMR AHMED AND ERIC P. XING *

School of Computer Science, Carnegie Mellon University

Stochastic networks are a plausible representation of the relational information among entities in dynamic systems such as living cells or social communities. While there is a rich literature in estimating a static or temporally invariant network from observation data, little has been done towards estimating time-varying networks from time series of entity attributes. In this paper, we present two new machine learning methods for estimating time-varying networks, which both build on a temporally smoothed l_1 -regularized logistic regression formalism that can be cast as standard convex-optimization problem and solved efficiently using generic solvers scalable to large networks. We report promising results on recovering simulated time-varying networks. For real datasets, we reverse engineer the latent sequence of temporally rewiring political network between Senators from the US senate voting records and the latent evolving gene network which contains more than 4000 genes from the life cycle of *Drosophila melanogaster* from microarray time course.

1. Introduction. Networks are a fundamental form of representation of information. In many problems arising in biology, social sciences and various other fields, it is often necessary to analyze populations of entities such as molecules or individuals, interconnected by a set of relationships (e.g., physical interactions or functional regulations in biological contexts, and friendship, communication, etc. in social contexts). Studying networks of these kinds can reveal a wide range of information, such as how molecules/individuals organize themselves into groups; which molecules are the key regulator or with individuals are in positions of power; and how the patterns of biological regulations or social interactions are likely to evolve over time. While there is a rich (and growing) literature on modeling a static network at a single point in time, or time-invariant networks, much less has been done toward modeling the dynamical processes underlying networks that are rewiring over time; and on developing learning techniques for recovering unobserved networks from time series of entity attributes. This structure estimation problem is especially important in the domains with very little prior knowledge about the existing interactions and relationships between actors. Once estimated, the structure of the network can be an-

*To whom corresponds should be addressed.

alyzed by an expert to obtain a better understanding of the underlying processes in nature. Many existing procedures for the structure estimation assume that the structure is static and that the observed data is independent and identically distributed. The assumption of the structure stability can be seen as inappropriate in, for example, analysis of stock prices where interactions between stocks change over time, or a biological experiment that measures gene expression levels during the developmental cycle of an organism. The focus of this paper is on the structure estimation of networks that evolve over time, and we restricted our analysis to undirected structures.

Formally, the relationships between actors in a given network can be concisely described by a graph $G(V, E)$, in which a node $a \in V$ denotes an actor; and an edge, $(a, b) \in E$, denotes a unidirectional (e.g., a contacted b) or symmetric (e.g., a and b are friends) relationship between a pair of actors in a complex system. Markov random fields (MRF) are an appropriate probabilistic model to represent these interactions. A Markov random field is specified by an undirected graph $G = (V, E)$, where $V = \{1, \dots, p\}$ is a vertex set and $E \subseteq V \times V$ is an edge set. Let $X = (X_1, \dots, X_p)^T$ be the p -dimensional random vector whose distribution P can be represented by the graph G . Each vertex from the set V is associated with one component of the random vector X . The edge set E of the graph G encodes certain conditional independence assumptions among subsets of the p -dimensional random vector X ; X_i is conditionally independent of X_j given the other variables if $(i, j) \notin E$.

The fundamental problem we are going to address is that of a graphic structure estimation: given a sample \mathcal{D}^n of size n from Markov random field, estimate the structure of the underlying graph. In this work, we will discard the assumption that the sample is independent and identically distributed (i.i.d.), and assume only that it is independent, i.e., instances can be drawn from possibly different MRF distributions. This relaxed assumption will allow us to estimate graphs with time varying structure.

There has been a great amount of work done in estimating graphs with static structure. Assume for the moment that we are given an independent and identically distributed sample of n data points $\mathcal{D}^n = \{x^{(i)} = (x_1^{(i)}, \dots, x_p^{(i)})\}_{i=1}^n$ from P . Under the assumption that X is a multivariate normal distribution with mean vector μ and covariance matrix Σ , estimation of the graph structure is equivalent to the estimation of zeros in the inverse covariance matrix $\Omega \equiv \Sigma^{-1}$ (Lauritzen, 1996), commonly referred to as the concentration matrix. Drton and Perlman (2004) proposed a method that tests for partial correlations that are not significantly different from zero, which can be applied when the number of dimensions p is small in

comparison to the sample size n . In recent years, there has been a surge of data sets that are high dimensional with few samples, e.g. data coming from microarray experiments and fMRI data. These “large p , small n ” data sets pose a difficult estimation problem, but under the assumption that the graph is sparse and the data is multivariate normal, several methods can be employed successfully for structure recovery. [Meinshausen and Bühlmann \(2006\)](#) proposed a procedure based on *neighborhood selection* of each node via the ℓ_1 penalized regression. Their procedure selects the model consistently under a set of suitable conditions, of which the most important one is commonly known in the literature as the irrepresentable condition ([Meinshausen and Bühlmann, 2006](#); [Wainwright, 2006](#); [Zhao and Yu, 2006](#)). [Peng et al. \(2008\)](#) propose a different neighborhood selection procedure for the structure estimation in which they estimate all neighborhoods jointly. The joint estimation procedure gives the global structure and improves on the neighborhood selection on a variety of networks. These methods based on the neighborhood selection are suitable for large-scale problems due to availability of fast solvers to ℓ_1 penalized problems ([Efron et al., 2004](#); [Friedman et al., 2007a](#)).

Another popular approach to the structure estimation is the ℓ_1 penalized likelihood, which achieves simultaneously model selection and parameter estimation. The penalized likelihood approach is much more computationally intensive since finding the estimate involves solving a semidefinite program (SDP) and a number of authors have worked on finding a more efficient way to solve the problem ([Banerjee et al., 2008](#); [Yuan and Lin, 2007](#); [Friedman et al., 2007b](#); [Duchi et al., 2008a](#); [Rothman et al., 2008](#)). Of these methods, it seems that the graphical lasso ([Friedman et al., 2007b](#)) is the most computationally efficient. Other than the ℓ_1 penalized likelihood estimation, some authors have proposed to use a non-concave penalty instead ([Fan and Li, 2001](#); [Fan et al., 2008](#); [Zou and Li, 2008](#)). This non-concave penalty tries to remedy the bias that the ℓ_1 penalty introduces.

If the random variable X is discrete, the problem of structure estimation becomes even more difficult since the likelihood cannot be optimized efficiently due to the problem of evaluation of the log-partition function. [Wainwright et al. \(2006\)](#) use a pseudo-likelihood approach, based on the local conditional likelihood at each node, similar to the neighborhood selection method of [Meinshausen and Bühlmann \(2006\)](#). This procedure results in a consistent neighborhood selection of each node, and hence in the consistent structure estimation.

On the other hand, with few exceptions ([Hanneke and Xing, 2006](#); [Sarkar and Moore, 2006](#); [Guo et al., 2007](#); [Zhou et al., 2008](#)), much less has been

done towards modeling dynamical processes that guide topological rewiring and semantical evolution of networks over time. Efficient techniques need to be developed for recovering unobserved network topologies from observed attributes of entities constituting the network. [Hanneke and Xing \(2006\)](#) proposed a new class of models, called *temporal Exponentially Random Graph Models* (tERGMs), for modelling networks evolving over discrete time steps. tERGM uses statistics like "edge-stability", "reciprocity", "density", and "transitivity" of time-adjacent graphs to construct a log-linear graph transition model $P(G^t|G^{t-1})$ that captures graph rewiring dynamics. Based on the tERGM, a *hidden tERGM* (htERGM) can be formulated to impose stochastic constraints on latent rewiring graphs. Similar to HMM, in principle one can infer time-specific network topology from the posterior distribution of G^t , given the time series of node attributes under htERGM ([Guo et al., 2007](#)). However, even though the htERGM is quite expressive, a Gibbs sampling algorithm for posterior inference is very inefficient and scales only to a few tens of nodes; developing a tractable algorithm for inference in the htERGM remains an open problem. Moreover, [Zhou et al. \(2008\)](#) develop a nonparametric method for estimation of the concentration matrix that varies smoothly over time. Their method produces a consistent estimate with the rate of convergence $\mathcal{O}_p\left(\sqrt{\frac{(p+s)\log n}{n^{2/3}}}\right)$, under a set of suitable assumptions.

With the avalanche of high-dimensional time-series data such as genome-wide gene expression time courses and large-scale social media streams, a key technical hurdle that prevents us from in-depth investigations of the mechanisms underlying these data, such as the dynamic gene regulation in developing organisms or the emergence/disingetration of cryptic liaisons and communities in society, is the unavailability of *serial snapshots* of the rewiring network during the progression of the process in question. Indeed, it is often technically impossible to determine time-specific network topologies in many natural or socio-cultural systems, and the only remaining option is to resort to computational-based statistical inference. With the current results reviewed above, there is an apparent gap between imminent methodological needs and the available data. In this paper, we narrow this gap by presenting two practical algorithms for estimating time-varying graphs.

The paper is organized as follows. In [Section 2](#) we describe the proposed models for estimation of the time varying graphical structures and the algorithms for obtaining the estimators. In [Section 3](#), the performance of the methods is demonstrated through simulation studies. In [Section 4](#), the methods are applied to some real world data sets. In [Section 5](#), we discuss some theoretical properties of the algorithms, however, the details are left for a separate paper. Discussion is given in [Section 6](#).

2. Methods. Let $X^t \sim P^t$ be a p dimensional random vector distributed according to some distribution P^t . We will assume that the distribution changes with the time index t and for convenience we choose to index time as $\mathcal{T}^n = \{1/n, 2/n, \dots, 1\}$. Given a sample of independent observations $\mathcal{D}^n = \{X^t \sim P^t \mid t \in \mathcal{T}^n\}$, the task is to estimate the undirected graph $G^t = (V, E^t)$ corresponding to the distribution P^t . Primarily, we will be interested in estimation of networks from “large p , small n “ data sets¹. The estimation problem is ill-posed, since there are more parameters than samples. To deal with the problem, we will assume that the true networks are sparse, or, at least, that the main interactions inside the network can be approximated with a sparse model. In many real data sets this sparsity assumption holds quite well. For example, in a genetic network, rarely a regulator gene would control more than a handful of regulatees under a specific condition (Davidson, 2001).

The estimation of the time varying networks is considered in two scenarios, which we formally define later: (a) the distribution P^t changes smoothly over time, (b) the distribution P^t is constant over periods of time with some sudden sharp changes. For the case (a), where the distribution P^t changes smoothly over time, we will use a nonparametric kernel estimate. In the case (b), the problem is to detect change points, the time points where the network exhibits sharp changes and estimate the network between change points. The case (b) is known as estimation with structural changes. We propose to use a total variation penalty which enforces similarity between parameters that are close in time. The total variation penalty has been successfully applied in detecting sharp transitions in signal processing, image denoising and nonparametric estimation, e.g Rudin et al. (1992); Mammen and Geer (1997); Davies and Kovac (2001). It has also been successfully applied to model selection in linear regression to identify blocks of nonzero coefficients Tibshirani et al. (2005); Friedman et al. (2007a).

In particular, we will be concerned with estimation of graphs from discrete data. This encompasses a large class of problems in practice. For instance, in social science, discrete data, such as movie rating data and senate voting data, are prevalent. Or in neural science, the sequence of action potentials from neurons can be view as discrete pulses. Or in biological science, measurements from microarray experiments are discretized to robustly capture the qualitative activity of the genes.

Formally, let X^t be a random vector taking its values in $\{-1, 1\}^p$ and let $G^t = (V, E^t)$ be its associated graph. For simplicity, we will consider

¹We allow dimension $p = p(n)$ to grow with the sample size n , however, we usually suppress this in our notation

binary Markov random fields (MRFs) with pairwise interactions, in which the probability distribution of X^t takes the form

$$(1) \quad \mathbb{P}_{\theta^{*,t}}(X) = \frac{1}{Z(\theta^{*,t})} \exp \left(\sum_{(u,v) \in E^t} \theta_{uv}^{*,t} x_u x_v \right),$$

where $Z(\theta)$ is the partition function that ensures that \mathbb{P} is a probability distribution and θ is the parameter vector. This type of MRF is known as the Ising model.

Let $\mathcal{D}^n = \{X^t \sim \mathbb{P}_{\theta^{*,t}} \mid t \in \mathcal{T}^n\}$ be an independent sample. Note that each sample X^t is coming from a different distribution $\mathbb{P}_{\theta^{*,t}}$ indexed by $\theta^{*,t}$ and that there is an undirected graph $G^t = (V, E^t)$ associated with it. It is going to be useful to consider the parameter vector $\theta^{*,t}$ as a $\binom{p}{2}$ -dimensional vector, indexed by distinct edges, and non-zero if and only if the edge $(u, v) \in E^t$. The problem of recovering the structure of the graph G^t is now equivalent to estimating non-zero elements of the vector $\theta^{*,t}$.

Estimation of the parameter vector $\theta^{*,t}$ by maximizing log-likelihood is not practically feasible due to the problem of evaluation of the log-partition function. One approach to overcoming this problem is to use a surrogate likelihood function which can be tractably optimized. However, for an estimate $\tilde{\theta}$, obtained through maximization of a surrogate likelihood, one cannot guarantee how close $\tilde{\theta}$ and $\theta^{*,t}$ are in general. That said, we have decided not to use the approach of [Banerjee et al. \(2008\)](#) to estimate discrete MRFs. Instead, we adapt the neighborhood selection procedure of [Wainwright et al. \(2006\)](#) to estimate time-varying MRFs.

We continue with a presentation of the algorithm for the structure recovery that is based on the neighborhood recovery of each node. Observe that recovering the edge set E^t of the graph G^t is equivalent to recovering, for each vertex $u \in V$, its neighborhood set $\mathcal{N}(u, t) = \{v \in V \mid (u, v) \in E^t\}$. The neighborhood set $\mathcal{N}(u, t)$ can be estimated from the sparsity pattern of the $(p-1)$ -dimensional subvector of parameters $\theta_{\setminus u}^{*,t} := \{\theta_{uv}^{*,t} \mid v \in V \setminus u\}$ associated with vertex u . Now, under the model (1), the conditional distribution of X_u^t given other variables $X_{\setminus u}^t$ takes the form

$$(2) \quad \mathbb{P}_{\theta^{*,t}}(x_u^t \mid x_{\setminus u}^t) = \frac{\exp \left(2x_u^t \langle \theta_{\setminus u}^{*,t}, x_{\setminus u}^t \rangle \right)}{\exp \left(2x_u^t \langle \theta_{\setminus u}^{*,t}, x_{\setminus u}^t \rangle \right) + 1},$$

where $\langle a, b \rangle = a^T b$ denotes dot product. The log-likelihood, for the node u ,

can be written in the following form:

$$(3) \quad \begin{aligned} \gamma(\theta^t; x^t) &= \log \mathbb{P}_{\theta^t}(x_u^t | x_{\setminus u}^t) \\ &= x_u^t \langle \theta_{\setminus u}^t, x_{\setminus u}^t \rangle - \log \left(\exp(\langle \theta_{\setminus u}^t, x_{\setminus u}^t \rangle) + \exp(-\langle \theta_{\setminus u}^t, x_{\setminus u}^t \rangle) \right). \end{aligned}$$

In the i.i.d. case, when the graph structure does not change over time, [Wainwright et al. \(2006\)](#) have considered an ℓ_1 penalized maximum likelihood approach for estimation of the signed neighborhood using (2). However, since we do not have identically distributed sample, we have to modify the approach. We are going to consider two types of changes: (a) in which the model changes smoothly over time and (b) where the model changes its structure at time points in the set \mathcal{T} .

2.1. Smooth changes for discrete MRFs. We start by describing how to estimate the neighborhood of the node u . For the point of interest $t_0 \in [0, 1]$, we define our estimator $\hat{\theta}$ as the solution to the following minimization problem:

$$(4) \quad \min_{\theta \in \mathbb{R}^{p_n-1}} \{l(\theta; \mathcal{D}^n) + \lambda_n \|\theta\|_1\}$$

where

$$(5) \quad l(\theta; \mathcal{D}^n) = - \sum_{t \in \mathcal{T}^n} w_t \gamma(\theta; x^t)$$

is a weighted logloss, with weights defined as $w_t = \frac{K_{h_n}(t-t_0)}{\sum_{t' \in \mathcal{T}^n} K_{h_n}(t'-t_0)}$ and $K_{h_n}(\cdot) = K(\cdot/h_n)$ is a kernel. The parameter $\lambda_n \geq 0$ is a regularization parameter specified by user that controls the size of the estimated neighborhood. The kernel $K_{h_n}(\cdot)$ is a symmetric nonnegative function.

Let $\hat{\theta}$ be a minimizer of (4). Based on the vector $\hat{\theta}$, we construct the estimate of the neighborhood:

$$(6) \quad \widehat{\mathcal{N}}(u, t_0) := \{v \mid v \in V \setminus u, \hat{\theta}_{uv} \neq 0\}.$$

Note that the procedure described above gives estimate only at the time point t_0 , so it is usually run for many time points to get insight into the structure dynamics. In the rest of this paper, we refer to this approach as **smooth**.

The optimization problem (4) is the well known objective of ℓ_1 penalized logistic regression and there are many ways of solving it. For completeness, we mention few scalable solutions. [Koh et al. \(2007\)](#) develop a specialized

interior point method for solving ℓ_1 penalized logistic regression. Using Lagrangian duality, problem (4) can be written in the equivalent constrained form

$$(7) \quad \min_{\|\theta\|_1 \leq C(\lambda_n)} \left\{ - \sum_{t \in \mathcal{T}^n} w_t \gamma(\theta; x^t) \right\},$$

for some constant $C(\lambda_n) < +\infty$. Similar to [Duchi et al. \(2008a\)](#), a subgradient descent algorithm with projection onto the ℓ_1 ball ([Duchi et al., 2008b](#)) solves the problem (7) very efficiently. To obtain results in this paper we use a fast coordinate-wise descent method described in [Friedman et al. \(2008\)](#). From our limited experience, the specialized first order method works faster than the interior point method.

The coordinate-wise descent method can be described schematically as

1. Set initial values

$$\hat{\theta}_{\setminus u,1}^{t_0,0}, \dots, \hat{\theta}_{\setminus u,p-1}^{t_0,0} \leftarrow 0$$

2. For $i = 1, \dots, p-1$, set the current estimate $\hat{\theta}_{\setminus u,i}^{t_0,iter+1}$ as a solution to the following optimization procedure

$$(8) \quad \min_{\theta \in \mathbb{R}} \left\{ \sum_{t \in \mathcal{T}^n} \gamma \left(\hat{\theta}_{\setminus u,1}^{t_0,iter+1}, \dots, \hat{\theta}_{\setminus u,i-1}^{t_0,iter+1}, \theta, \hat{\theta}_{\setminus u,i+1}^{t_0,iter}, \dots, \hat{\theta}_{\setminus u,p-1}^{t_0,iter}; \mathcal{D}^n \right) + \lambda_1 |\theta| \right\}.$$

3. Repeat step 2 until convergence

For efficient way of solving (8) refer to [Friedman et al. \(2008\)](#).

2.2. Structural changes in discrete MRFs. While most phenomena in real life change smoothly, the rate at which we observe them might not reveal this smooth change. Indeed, while most edges in a given network evolve (appear or disappear) smoothly over time, the sampling rate might give the impression that some of these edges change abruptly. This abrupt change violates some of the assumptions of the `smooth` method (see Appendix). In this section, we investigate a different approach, which we will call `TV`, that is suitable for recovering abruptly changing networks.

We propose to estimate the neighborhood of the node u by solving the following optimization problem

$$(9) \quad \hat{\theta}_{\setminus u}^t = \operatorname{argmin}_{\theta \in \mathcal{F}^{p-1}} \left\{ \sum_{t \in \mathcal{T}^n} \gamma(\theta^t; x^t) + \lambda_1 \sum_{t \in \mathcal{T}^n} \|\theta^t\|_1 + \lambda_2 \sum_{v \in V \setminus u} TV(\theta_v^t) \right\}.$$

Here $\mathcal{F}^{p-1} = \{(f_1, f_2, \dots, f_{p-1})^T \mid f_i \in \mathcal{F}_{\mathcal{T}^n}^0\}$ is a class of functions over which we are optimizing and $\mathcal{F}_{\mathcal{T}}^0$ is class of univariate functions defined on

$[0, 1]$ that are piecewise constant and right continuous, with discontinuities in the set \mathcal{T} . It is worth noting that the solution to problem (9) gives estimate of the neighborhood for node u for every time t , and not just for the time t_0 as was the case in (4).

The penalty is structured as a combination of two terms. The first term penalizes the complexity of the neighborhood estimate at each time point in \mathcal{T}^n and the tuning parameter λ_1 regulates the size of the estimated neighborhood. The second term penalizes the difference between coefficients that are adjacent in time and, as a result, biases the estimate towards functions that are “blocky.” This composite penalty was also successfully applied in a slightly different setting of linear regression with correlated covariates, where it is known as the “fused” lasso penalty (Tibshirani et al., 2005).

The optimization problem (9) is convex and hence it can be solved efficiently, however, it is more complex than problem (4) and we do not know of any specialized algorithms that can be used to solve it. Here we spend some time discussing the optimization procedure for problem (9), which turned out to be much more efficient than the existing “off the shelf” solvers.

We start from the observation that the loss function can be factorized as $\mathcal{L}(\theta) = h(\theta_1, \theta_2, \dots, \theta_p) + \sum_{i=1}^p g(\theta_i)$ for some functions h and g . Tseng (2001) established that the block-coordinate descent converges for the loss functions with such structure, where h is differentiable and g is convex. Based on this observation we propose the following algorithm:

1. Set initial values

$$\hat{\theta}_{\setminus u,1}^{i,0}, \dots, \hat{\theta}_{\setminus u,p-1}^{i,0} \leftarrow 0$$

2. For $i = 1, \dots, p - 1$, set the current estimate $\hat{\theta}_{\setminus u,i}^{i,iter+1}$ as a solution to the following optimization procedure

$$(10) \quad \min_{\theta \in \mathcal{F}_{\mathcal{T}^n}^0} \left\{ \begin{array}{l} \sum_{t \in \mathcal{T}^n} \gamma \left(\hat{\theta}_{\setminus u,1}^{i,iter+1}, \dots, \hat{\theta}_{\setminus u,i-1}^{i,iter+1}, \theta^t, \hat{\theta}_{\setminus u,i+1}^{i,iter}, \dots, \hat{\theta}_{\setminus u,p-1}^{i,iter}; \mathcal{D}^n \right) \\ + \lambda_1 \sum_{t \in \mathcal{T}^n} |\theta^t| \\ + \lambda_2 TV(\theta^t) \end{array} \right\}.$$

3. Repeat step 2 until convergence

Using the proposed block-coordinate descent algorithm, we solve a sequence of optimization problems (10) with n variables, instead of solving one big $n * (p - 1)$ optimization problem (9). In practice, this gives us a faster algorithm and we are able to solve larger problems. It is still an open question how to solve (10) in the most efficient way, however we do not pursue it here. For the problems considered in this paper, it is sufficient to use the optimization package CVX (Grant and Boyd, 2008) to solve for (10).

2.3. *Multiple observations.* In the presentation of the two algorithms, we have assumed that at each time point in \mathcal{T}^n there is only one observation. It can be easily imagined that there are multiple samples at each time point, e.g. a controlled repeated micro-array experiment in which two samples obtained at certain time points could be regarded as independent and identically distributed. Here, we describe how one can easily adapt the two procedures to this setting and later, in Section 3, we show how the estimation procedure benefits from additional observations at each time point.

There are virtually no modifications needed to accommodate multiple observations at different time points in Equation (4). Each additional sample will be assigned the same weight through the kernel function $K_{h_n}(\cdot)$. Only one small change is needed to modify Equation (9) which becomes

$$(11) \hat{\theta}_{\setminus u}^t = \operatorname{argmin}_{\theta \in \mathcal{F}^{p-1}} \left\{ \sum_{t \in \mathcal{T}^n} \sum_{x \in \mathcal{D}^{n,t}} \gamma(\theta^t; x) + \lambda_1 \sum_{t \in \mathcal{T}^n} \|\theta^t\|_1 + \lambda_2 \sum_{v \in V \setminus u} TV(\theta_v^t) \right\}.$$

The set $\mathcal{D}^{n,t}$ denotes elements from sample \mathcal{D}^n observed at time point t .

2.4. *Choosing tuning parameters.* Both algorithms for estimating network with smooth changes (**smooth**) and for estimating network with structural changes (**TV**) require a choice of tuning parameters. These tuning parameters control sparsity of estimated networks and rate at which network changes over time. For both methods, the sparsity of estimates is controlled with the penalty parameter λ_1 . Rate of change is controlled through the bandwidth parameter h_n in the method **smooth** and with the penalty parameter λ_2 in the method **TV**. Choosing the tuning parameters is of extreme importance in getting a good estimate that does not overfit the data. Large values of the penalty parameter λ_1 result in a sparse estimate, while small values result in a dense model that has higher log-likelihood, but more degrees of freedom. The bandwidth parameter h_n controls smoothness of estimated networks in **smooth** method; small values give estimates that change often over time, and large values result in estimates that are almost time invariant. Intuitively, the bandwidth parameter can be thought of as a size of the neighborhood of samples that are used to construct a network at time point t_0 . The penalty parameter λ_2 controls the smoothness in a slightly different way; large values penalize the difference between parameters adjacent in time and bias solution towards a network that is slowly changing, while small values allow for more changes in estimates.

To tune these parameters, one should first note that $\gamma(\theta^t; x^t)$ in both (9) and (4) represents a logistic regression loss function for each node, thus each of (9) and (4) can be regarded as a *supervised* classification problem

where each node u is regressed on the other nodes $V \setminus u$. Many techniques can be used to select the tuning parameters among different candidates. When there are enough data, cross-validation, or held-out datasets can be used, otherwise, the BIC score can be employed. We define the BIC score for $(\theta_{\setminus u}^1, \dots, \theta_{\setminus u}^{\mathcal{T}^n})$ to be

$$(12) \quad \text{BIC}(\theta_{\setminus u}^1, \dots, \theta_{\setminus u}^{\mathcal{T}^n}) \approx \sum_{t=1}^{\mathcal{T}^n} \sum_{x \in \mathcal{D}^{n,t}} \gamma(\theta^t; x) - \frac{\log(\sum_{t=1}^{\mathcal{T}^n} \mathcal{D}^{n,t})}{2} \text{Dim}(\theta_{\setminus u}^1, \dots, \theta_{\setminus u}^{\mathcal{T}^n}),$$

where $\text{Dim}(\cdot)$ denotes the dimensionality of the estimated parameters. Similar to [Tibshirani et al. \(2005\)](#), we adopt the following definition which counts the number of runs of non-zero parameter values

$$(13) \quad \text{Dim}(\theta_{\setminus u}^1, \dots, \theta_{\setminus u}^{\mathcal{T}^n}) = \sum_{t=1}^{\mathcal{T}^n} \sum_{v \in V} I[\text{sign}(\theta_{uv}^t) \neq \text{sign}(\theta_{uv}^{t-1})] \times I[\text{sign}(\theta_{uv}^t) \neq 0].$$

Note that the above definition is lenient to perturbations to the value of the actual parameters, whereas the definition in [Tibshirani et al. \(2005\)](#) strictly increases the dimensionality of the model with these perturbations. Our intuition here is that a non-zero parameter corresponds to an edge, thus the measure in (13) counts the number of edge changing events including change in polarity. The BIC score in (12) can be applied to each node independently which allows for nodes to have neighborhoods of different sizes and different rates of change for these neighborhoods.

In the kernel reweighting approach, the tuning of bandwidth parameter h_n should trade off the smoothness of the network changes and the coverage of samples used to estimate the network. Using a wider bandwidth parameter provides more samples to estimate the network, but this risks missing sharper changes in the network; using a narrower bandwidth parameter makes the estimate more sensitive to sharper changes, but this also makes the estimate subject to larger variance due to the reduced effective sample size. In this paper, we adopt a heuristic for tuning the initial scale of the bandwidth parameter: we set it to be the median of the distance between pairs of time points. That is, we first form a matrix (d_{ij}) with its entries $d_{ij} := (t_i - t_j)^2$ ($t_i, t_j \in \mathcal{T}^n$). Then the scale of the bandwidth parameter is set to the median of the entries in (d_{ij}) . In our later simulation experiments, we find that this heuristic provides a good initial guess for h_n , and it is quite close to the value obtained via more exhaustive search.

3. Simulation studies. In this section, we perform experiments on simulated data to assess the performance of the proposed methods. The experiments are conducted in a way to give insight on when to use the kernel smoothing method, which we denote `smooth`, and when to use the method based on the total variation penalty, which we denote `TV`. It is also instructive to compare these two methods with the neighborhood selection method which assumes that the graph is time invariant [Wainwright et al. \(2006\)](#), which we denote `static`. For a given time point $t_0 \in [0, 1]$, all three methods produce two estimates $\tilde{\theta}_{uv}$ and $\tilde{\theta}_{vu}$ for each edge parameter. This is the artifact of the algorithms in which neighborhoods for nodes u and v are estimated separately. There are two ways to symmetrize the solution:

$$\hat{\theta}_{uv} = \begin{cases} \tilde{\theta}_{uv} & \text{if } |\tilde{\theta}_{uv}| < |\tilde{\theta}_{vu}| \\ \tilde{\theta}_{vu} & \text{if } |\tilde{\theta}_{uv}| \geq |\tilde{\theta}_{vu}| \end{cases} \quad \text{“min_symmetrization”},$$

and

$$\hat{\theta}_{uv} = \begin{cases} \tilde{\theta}_{uv} & \text{if } |\tilde{\theta}_{uv}| > |\tilde{\theta}_{vu}| \\ \tilde{\theta}_{vu} & \text{if } |\tilde{\theta}_{uv}| \leq |\tilde{\theta}_{vu}| \end{cases} \quad \text{“max_symmetrization”}.$$

For each of the three methods, we will denote the solutions obtained through different symmetrization as `****.MIN` and `****.MAX`.

We simulate our data from a random network, which is generated using the following procedure. The network has p nodes that are connected with e randomly added edges between pairs of nodes. The edges are added in such a way that the maximum degree of a node is d . Next, each edge $uv \in E$ is assigned the potential θ_{uv}^* uniformly at random from the interval $[\theta_{\min}, \theta_{\max}]$. This procedure creates the initial network. In addition, we consider two methods for generating time evolving network. The first method generates a network that smoothly evolves over time, while the second one generates a network that is piecewise constant.

To simulate the smoothly evolving network, we randomly choose `#change` edges to delete from the graph and randomly choose `#change` edges to add to the graph. For the edges to be added to the graph we also assign random potentials. The potentials of the edges are gradually decreased to zero or increased to the randomly assigned value over a period of `time_change` discrete time steps. This process of adding and removing edges is repeated several times. At each discrete time step we draw `num_iid` independent samples from the network using the Gibbs sampling. Note that using this procedure results in networks that almost always have $e + \text{\#change}$ edges.

The piecewise constant network is simulated in a similar fashion as a smoothly evolving one. The main difference is that we do not add and remove edges over a period of discrete time steps, instead, the network is kept

constant for *time_change* discrete time steps and then the edges are added and removed to the network.

We evaluate the estimation procedures by estimating the network at 9 time steps $\mathcal{T} = \{0.1, 0.2, \dots, 0.9\}$. We express our results in terms of F1 score, which is computed as $\frac{2 * P * R}{P + R}$ with P denoting precision and R denoting recall. Let \hat{E}^t denote the estimated edge set in \hat{G}^t . Precision is calculated as $\frac{|\hat{E}^t \cap E^t|}{|\hat{E}^t|}$ and recall as $\frac{|\hat{E}^t \cap E^t|}{|E^t|}$. The F1 score is a natural choice of the accuracy measure as it tries to balance between precision and recall.

3.1. Simulation of smoothly varying networks. We generate the initial random graph with $p = 20$ nodes and $e = 15$ edges. Each node of the graph has at most $s = 4$ neighbors. Parameters θ_{uv} for each edge is drawn uniformly at random from $[0.5, 1]$. Next, we randomly add 10 edges to the graph and choose 10 edges to remove from the graph. These edges are added and removed from the graph over 100 discrete time steps. At each discrete time step we generate *num_iid* i.i.d. samples. In our experiments, the parameter *num_iid* is going to be changed from 1 to 10. We repeat the process of adding and removing edges 5 times, so in total we simulate the changing network over 500 discrete time steps. On average our network has 25 edges. We report results averaged over 20 independent runs.

The choice of the tuning parameter λ_1 and the bandwidth h_n is of extreme importance for the estimation procedure. The number of edges included in the graph is controlled with the parameter λ_1 . As λ_1 increases, the estimated graph gets sparser. For the case with large λ_1 , the estimated graph is sparse and we have large precision, however, the recall is very low. On the other hand, with small λ_1 , the estimated graph contains many spurious edges and while recall is high, the precision is quite low. A good choice of the parameter λ_1 will balance the two extremes and result in a good F1 score. The bandwidth h_n controls the weight given to points in the neighborhood of time t for which we want to estimate a graph. The larger the bandwidth, the more points that are included in the neighborhood and the resulting estimate does not reflect the changes in the network, i.e. the solution is undersmoothed. If the bandwidth h_n is too small, only few points are included in the neighborhood and the resulting estimate is very unstable, i.e. the solution is oversmoothed. A similar role is played by the tuning parameters λ_1 and λ_2 in the TV procedure. The parameter λ_2 can be thought of as a parameter that controls the number of “blocks“ that solution consists of. In each of these blocks, the network does not change, and so implicitly the parameter λ_2 controls the size of the neighborhood, similarly to the way that the bandwidth parameter h_n controls the size of the neighborhood in

the `smooth` procedure.

Here, in the simulation experiments, we choose the bandwidth parameter as explained in Section 2.4. We run the algorithm over a grid of parameters, (λ_1, h_n) for `smooth` procedure and (λ_1, λ_2) for TV procedure, and choose one that optimizes the BIC-type criterion.

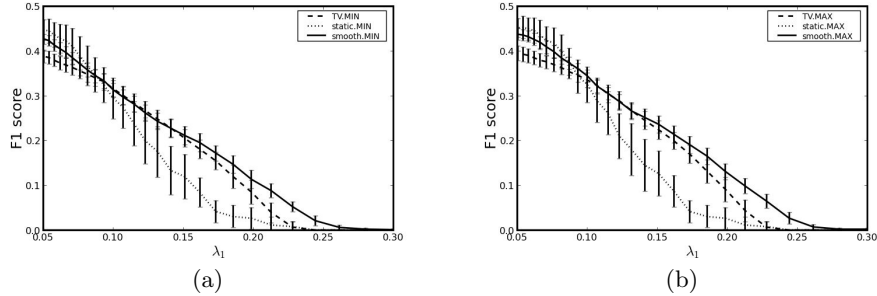


FIG 1. *Smoothly changing network. F1 score as a function of λ_1 . At each time step there were $\text{num_iid} = 1$ independent samples. The bandwidth parameter was set to $h_n = 0.182$. The TV parameter was set to $\lambda_2 = 0.223$.*

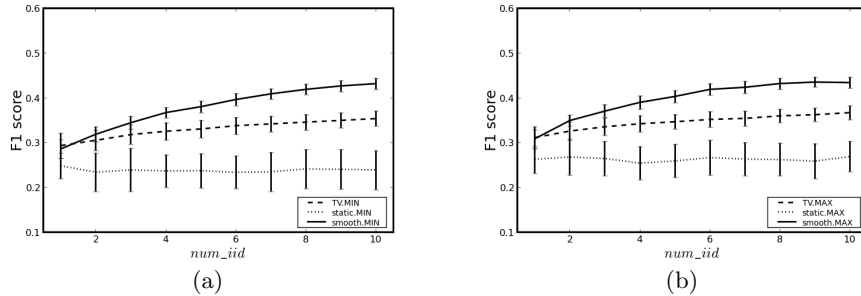


FIG 2. *Smoothly changing network. F1 score as a function of the number of independent samples at each discrete time step num_iid .*

We start by reporting results for a fixed bandwidth h_n and a fixed penalization parameter λ_2 . The results are given in Figure 1 as a function of the penalization parameter λ_1 . The fixed value of tuning parameters is somewhat arbitrary as we have used values close to the values picked by a BIC-type criterion, however, the aim of these plots is to give intuition on how F1 score varies with respect to the tuning parameter λ_1 . From Figure 1 we can see that the `smooth` method performs better than TV, which in turn performs better than the `static` method for most of the range of tuning

parameters λ_1 . The reason for small values of the penalty parameter λ_1 all methods perform alike is that the estimated graph is too dense and using an automatic method for picking λ_1 never chooses values from this region. As expected, `smooth` outperforms `TV` on the smoothly varying network, mainly because `TV` estimates a solution with many blocks and implicitly, as a result, estimates network from a small local neighborhood with few samples. It is worth noting that the performance of the `static` method degrades if the simulation is carried over a large number of time steps, which comes with no surprise as the static model assumption gets more violated.

Figure 2 represents F1 score averaged over 20 runs as a function of number of independent samples at each time step. Note that the performance of both methods `smooth` and `TV` increases with the sample size.

There are some differences between the estimates obtained through `MIN` and `MAX` symmetrization. In our limited numerical experience, we have seen that `MAX` symmetrization outperforms `MIN` symmetrization. `MIN` symmetrization is more conservative in including edges to the graph and seems to be more susceptible to noise.

3.2. Simulation of piecewise constant networks. To generate data from a piecewise constant network, we generate the initial random graph with $p = 20$ nodes and $e = 25$ edges, with constraint that each node has at most $s = 4$ neighbors. Parameters θ_{uv} for each edge are drawn uniformly at random from $[0.5, 1]$. We generate samples from this graph over 100 discrete time steps, at each step drawing num_iid i.i.d. samples, where num_iid ranges from 1 to 10. Next, we randomly remove 10 edges and add 10 edges to the graph and repeat the process of drawing samples over 100 discrete time steps. The process of changing graph is repeated 5 times, so that at the end we have simulated a network over 500 discrete time steps. We report results averaged over 20 independent runs.

Figure 3 gives F1 score as a function of the penalization parameter λ_1 , for fixed values of the other tuning parameters. For the piecewise constant network, we can see that the `TV` method tends to do better than `smooth` method. The reason is that `TV` estimates jumps relatively accurately and the solution is not affected with the structural changes in the model. On the other hand, `smooth` tends to suffer when the network is estimated at a point close to a change point since samples from both sides of the change are included into a neighborhood. As we increase sample size at each time step, Figure 4 shows the performance of the methods. We would like to emphasize here that the `TV` method fits the network at 500 different time points, at every discrete time point. However, for the comparison with the `smooth` method,

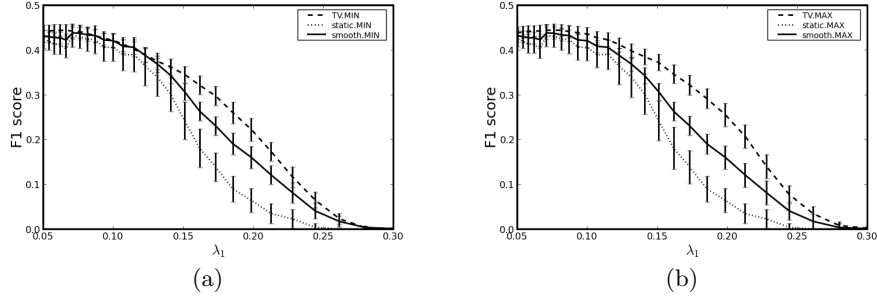


FIG 3. Piecewise constant network. $F1$ score as a function of λ_1 . At each time step there were $\text{num_iid} = 1$ independent samples. The bandwidth parameter was set to $h_n = 0.182$. The TV parameter was set to $\lambda_2 = 0.223$.

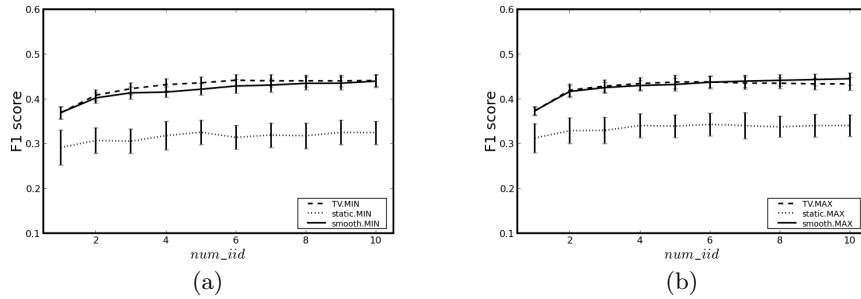


FIG 4. Piecewise constant network. $F1$ score as a function of the number of independent samples at each discrete time step num_iid .

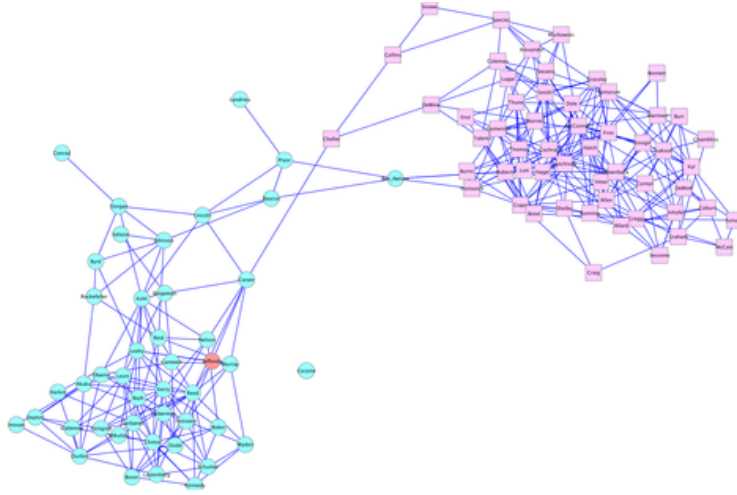


FIG 5. 109th Congress, Connections between Senators in April 2005.

we only evaluate network topology at time points $\mathcal{T} = \{0.1, 0.2, \dots, 0.9\}$. This decision affects the final result, since the network is constant at most of these points, and the two methods seem equivalent. While the TV method is able to estimate changes in the network, the `smooth` method performs somewhat unpredictable close to change points.

4. Experiments. In this section we present the analysis of two real data sets using the algorithms presented in Section 2. First, we present the analysis of the senate data consisting of Senators' votes on bills during the 109th Congress. The second data set consists of expression levels of more than 4000 genes from the life cycle of *Drosophila melanogaster*.

4.1. *Senate Voting Records Data.* The US senate data consists of voting records from 109th congress (2005 - 2006)². There are 100 senators whose votes were recorded on the 542 bills. Each senator corresponds to a variable, while the votes are samples recorded as -1 for no and 1 for yes. This data set was analyzed in Banerjee et al. (2008), where a static network was estimated. Here, we analyze this data set in a time varying framework in order to discover how the relationship between senators changes over time.

This data set has many missing values, corresponding to votes that were not cast. We follow the approach of Banerjee et al. (2008) and fill those missing values with (-1). Bills we mapped onto a $[0, 1]$ interval, with 0 representing Jan 1st, 2005 and 1 representing Dec 31st, 2006. To estimate the

²The data can be obtain from the U.S. Senate web page <http://www.senate.gov>

network we have chosen the bandwidth parameter to be $h_n = 0.174$ and the penalty parameter $\lambda_1 = 0.195$ for the method `smooth`, and penalty parameters $\lambda_1 = 0.24$ and $\lambda_2 = 0.28$ for the method `TV`. In our figures, square nodes represent republicans and circle nodes represent democrats.

At any time point t , the estimated network contains few clusters of nodes. These clusters consist of either Republicans or Democrats connected to each others (see Figure 5). There are few links connected to different clusters, as well as isolated Senators. This observation supports our intuition that most senators vote similarly to other members of their party. Links connecting different clusters usually go through senators that are members of one party, but have views more similar to the other party, e.g. Senator Ben Nelson or Senator Chafee. We do not necessarily need to estimate a time evolving network, as these simple observations can be seen from an estimate obtained using a procedure that estimates a static network (e.g. Banerjee et al. (2008)).

We are more interested in finding a time evolving pattern. First, we examine a neighborhood of the node representing Senators Corzine and Menendez. Senator Jon Corzine stepped down from the Senate at the end of the 1st Session in the 109th Congress to become the Governor of New Jersey. His place in the Senate was filled by Senator Bob Menendez. In our network, we have one node representing both senators, so at the end of the 1st Session we would expect to see some changes in the network, even though both senators are Democrats. Figure 6 presents first neighbors of the node at four different time steps, two during each Session. Note that this observation could not be seen from a static network.

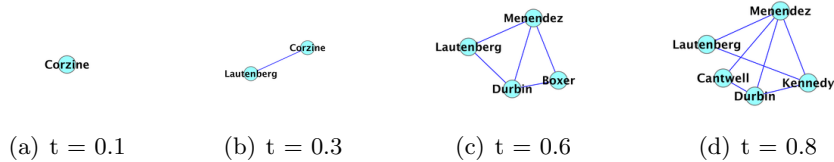


FIG 6. *Neighbors of the node that represents Senator Corzine and Senator Menendez at four different time points*

Next, we move onto the analysis of the neighbors of Senator Ben Nelson. Senator Ben Nelson is a Democrat from Nebraska and is considered as one of the most conservative Democrats in the Senate. Figure 7 presents neighbors of Senator Ben Nelson of degree two or less at two time points, one during the 1st Session and one during the 2nd Session. As a conservative Democrat, we expect him to have some Democrat and some Republican neighbors since

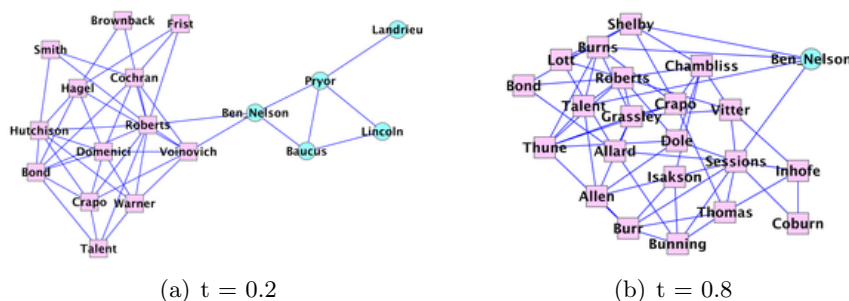


FIG 7. *Neighbors of Senator Ben Nelson (degree two or lower) at the beginning of 109th Congress and at the end of 109th Congress*

he shares views with both parties. This observation is supported by Figure 7(a) which presents his links during the 1st Session. It is also interesting to note that during the second session, his views drifted more towards the Republicans (Figure 7(b)). More detailed analysis of the type of bills passed during that period of time should be performed to explain this observation. We try to explain the observation by noting his political views on abortion, where he stands as a pro-life Democrat, and his political views on Iraq, in which he stood against withdrawal of most of the combat troops from Iraq.

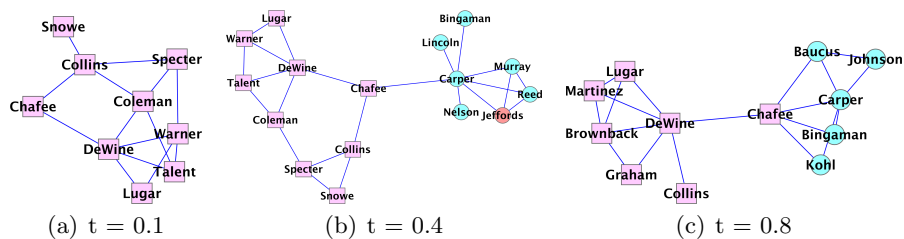


FIG 8. *Neighbors of Senator Chafee (degree two or lower)*

We report the results of the method TV in analysis of neighbors of Senator Lincoln Chafee. Figure 8 presents neighbors of Senator Chafee at three time points during the 109th Congress. We make a tentative observation that his neighborhood includes an increasing amount of Democrats as the graph is estimated at a later stage during the 109th Congress. Senator Chafee left the Republican Party and became an independent in 2007. Also, his view on abortion, gay rights and environmental policies are strongly aligned with those of Democrats, which supports behavior seen in the estimated network. Again, these observations could not be made if a static network

was estimated.

4.2. *Gene Regulatory Networks of Drosophila Melanogaster.* In this section, we used the kernel reweighting approach to reverse engineer the gene regulatory networks of *Drosophila melanogaster* from a time series of gene expression data measured during its full life cycle. Over the developmental course of *Drosophila melanogaster*, there exist multiple underlying “themes” that determine the functionalities of each gene and their relationships to each other, and such themes are dynamical and stochastic. As a result, the gene regulatory networks at each time point are context-dependent and can undergo systematic rewiring, rather than being invariant over time. In a seminal study by [Luscombe et al. \(2004\)](#), it was shown that the “active regulatory paths” in the gene regulatory networks of *Saccharomyces cerevisiae* exhibit topological changes and hub transience during a temporal cellular process, or in response to diverse stimuli. We expect similar properties can also be observed for the gene regulatory networks of *Drosophila melanogaster*.

We used microarray gene expression measurements from [Arbeitman et al. \(2002\)](#) as our input data. In such an experiment, the expression levels of 4028 genes are simultaneously measured at various developmental stages. Particularly, 66 time points are chosen during the full developmental cycle of *Drosophila melanogaster*, spanning across four different stages, *i.e.* embryonic (1–30 time point), larval (31–40 time point), pupal (41–58 time points) and adult stages (59–66 time points). In this study, we focused on 588 genes that are known to be related to developmental process based on their gene ontologies.

Usually, the samples prepared for microarray experiments are a mixture of tissues with possibly different expression levels. This means that microarray experiments only provide rough estimates of the average expression levels of the mixture. Other sources of noise can also be introduced into the microarray measurements during, for instance, the stage of hybridization and digitization. Therefore, microarray measurements are far from the exact values of the expression levels, and it will be more robust if we only consider the binary state of the gene expression: either being up-regulated or down-regulated. For this reason, we binarize the gene expression levels into $\{0, 1\}$ (-1 for down-regulated and 1 for up-regulated). We learned a sequence of binary MRFs from these time series.

In [Figure 9\(a\)](#), we plotted two different statistics of the reversed engineered gene regulatory networks as a function of the developmental time point (1–66). The first statistic is the network size as measured by the number of edges; and the second is the average local clustering coefficient as

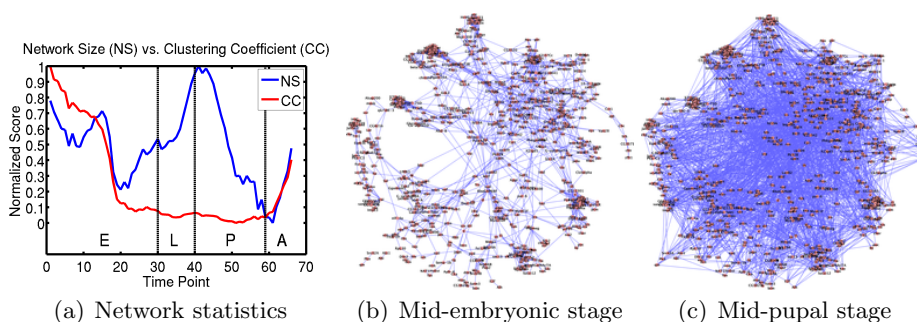


FIG 9. *Characteristic of the dynamic networks estimated for the genes related to developmental process. (a) Plot of two network statistics as functions of development time line. (b) and (c) visualization of two example of networks from different time point. We can see that network size can evolve in a very different way from the local clustering coefficient.*

defined by [Watts and Strogatz \(1998\)](#). For comparison, we normalized both statistics to the range between $[0, 1]$. It can be seen that the network size and its local clustering coefficient follow very different trajectories during the developmental cycle. The network size exhibits a wave structure featuring two peaks at mid-embryonic stage and the beginning of pupal stage. Similar pattern of gene activity has also been observed by [Arbeitman et al. \(2002\)](#). In contrast, the clustering coefficients of the dynamic networks drop sharply after the mid-embryonic stage, and they stays low until the start of the adult stage. One explanation is that at the beginning of the development process, genes have a more fixed and localized function, and they mainly interact with other genes with similar functions; however, after mid-embryonic stage, genes become more versatile and involved in more diverse roles to serve the need of rapid development; as the organism turns into an adult, its growth slows down and each gene is restored to its more specialized role. To illustrate how the network properties change over time, we visualized two networks from mid-embryonic stage (time point 15) and mid-pupal stage (time point 45) in Figure 9(b) and 9(c) respectively. Although the size of the two networks are comparable, we can see that there are much more clear local cluster of interacting genes during mid-embryonic stage.

To judge whether the learned networks make sense biologically, we zoom into three groups of genes functionally related to different stages of development process. In particular, the first group (30 genes) is related to embryonic development based on their functional ontologies; the second group (27 genes) is related to post-embryonic development; and the third group (25 genes) is related to muscle development. We used interactivity, which

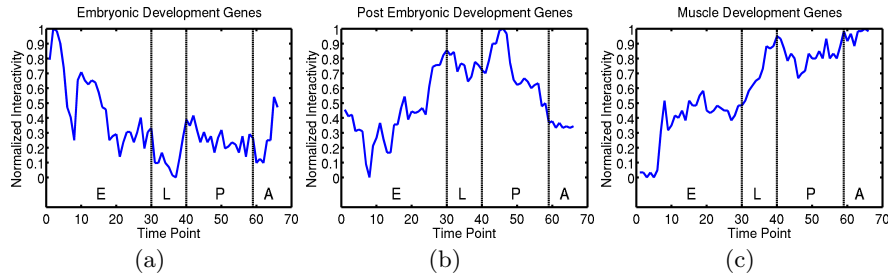


FIG 10. *Interactivity of 3 groups of genes related to (a) embryonic development; (b) post-embryonic development and (c) muscle development. The higher the interactivity, the more active the group of genes. We see that the interactivity of the three groups is very consistent with their functional annotation.*

is the total number of edges a group of genes is connected to, to describe the activity of each group genes. In Figure 10, we plotted the time courses of interactivity for the three groups respectively. For comparison, we normalize all scores to the range of $[0, 1]$. We see that the time courses have a nice correspondence with their supposed roles. For instance, embryonic development genes have the highest interactivity during embryonic stage, and post-embryonic genes increase their interactivity during larval and pupal stage. The muscle development genes are less specific to certain developmental stages, since they are needed across the developmental cycle. However, we see its increased activity when the organism approaches its adult stage where muscle development becomes increasingly important.

The estimated networks also recover many known interactions between genes. In recovering these known interactions, the dynamic networks also provide additional information as to when interactions occur during development. In Figure 11, we listed these recovered known interactions and the precise time when they occur. This also provides a way to check whether the learned networks are biologically plausible given the prior knowledge of the actual occurrence of gene interactions. For instance, the interaction between genes *msn* and *dock* is related to the regulation of embryonic cell shape, correct targeting of photoreceptor axons. This is very consistent with the timeline provided by the dynamic networks. A second example is the interaction between genes *sno* and *Dl* which is related to the development of compound eyes of *Drosophila*. A third example is between genes *caps* and *Chi* which are related to wing development during pupal stage. What is most interesting is that the dynamic networks provide timelines for many other gene interactions that have not yet been verified experimentally. This

information will be a useful guide for future experiments.

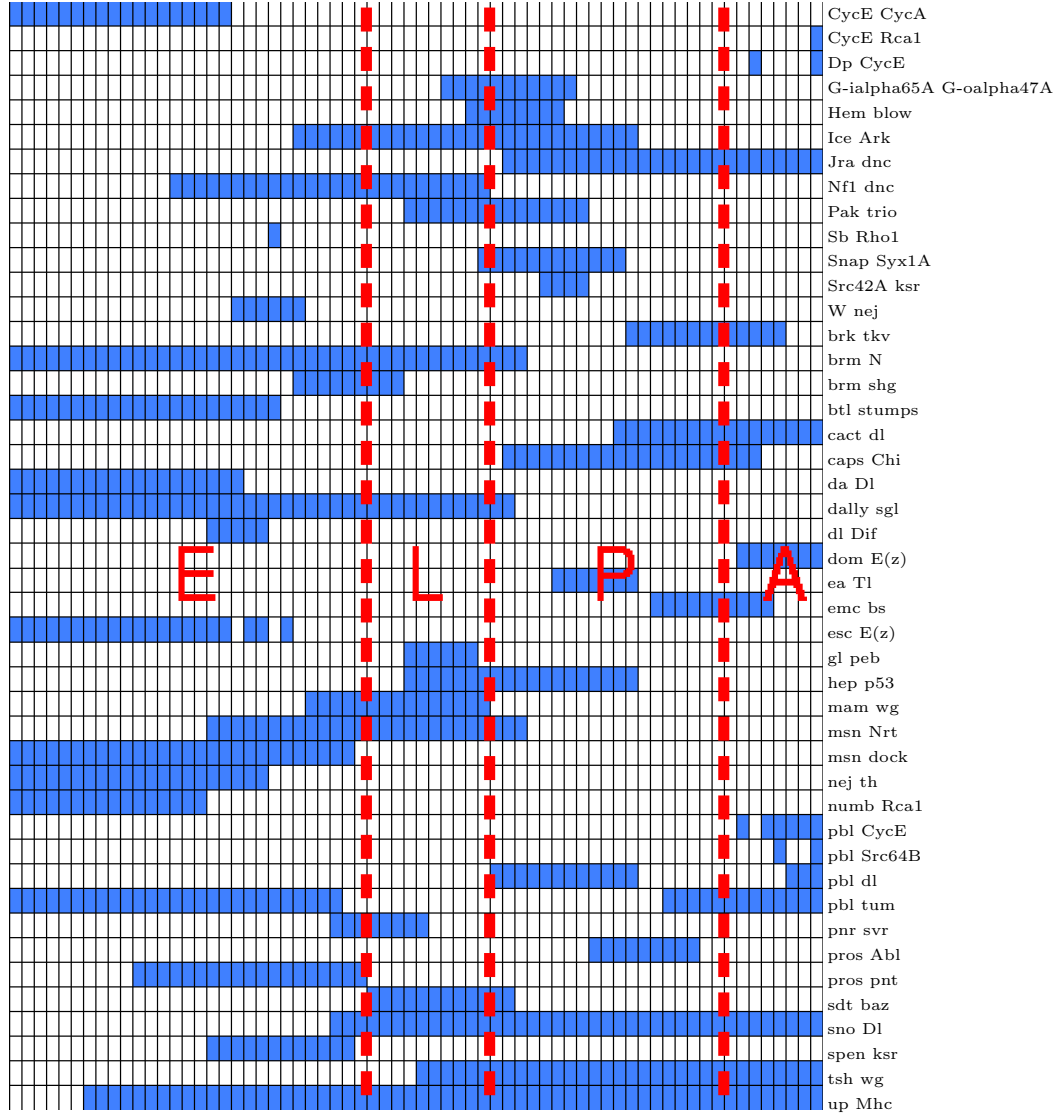


FIG 11. Timeline of 45 known gene interactions. Each cell in the plot corresponds to one gene pair of gene interaction at one specific time point. The cells in each row are ordered according to their time point, ranging from embryonic stage (E) to larval stage (L), to pupal stage (P), and to adult stage (A). Cells colored blue indicate the corresponding interaction listed in the right column is present in the estimated network; blank color indicates the interaction is absent.

We further studied the relations between 130 transcriptional factors (TF).

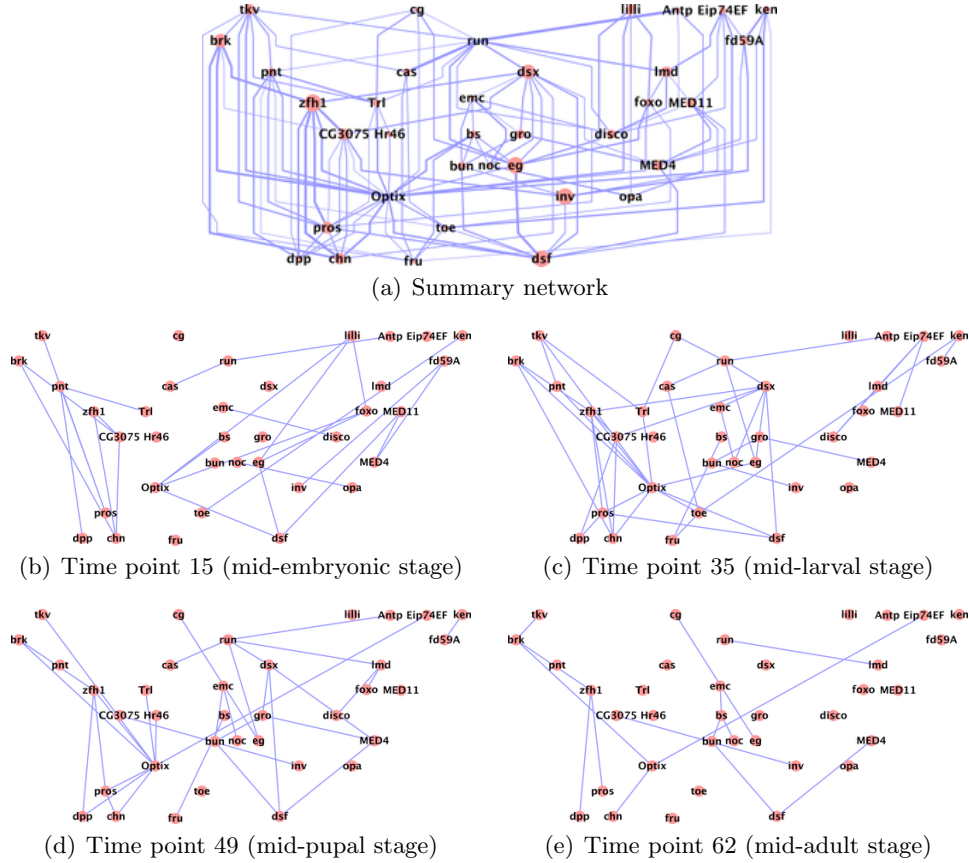


FIG 12. *The largest transcriptional factors (TF) cascade involving 36 transcriptional factors. (a) The summary network is obtained by summing the networks from all time points. Each node in the network represents a transcriptional factor, and each edge represents an interaction between them. The width of an edge is proportional to the number of the times the edge is present during the development; the size of a node is proportional to the sum of its edge weights. During different stages of the development, the networks are different, (b,c,d,e) shows representative networks for the embryonic, larval, pupal and adult stage of the development respectively.*

The network contains several cluster of transcriptional cascades, and we will present the detail of the largest transcriptional factor cascade involving 36 transcriptional factors (Figure 12). This cascade of TFs is functionally very coherent, and many TFs in this network play important roles in the nervous system and eye development. For example, Zn finger homeodomain 1 (zhf1), brinker (brk), charlatan (chn), decapentaplegic (dpp), invected (inv), forkhead box, subgroup 0 (foxo), Optix, eagle (eg), prospero (pros), pointed

(pnt), thickveins (tkv), extra macrochaetae (emc), lilliputian (lilli), double-sex (dsx) are all involved in nervous and eye development. Besides functional coherence, the networks also reveals the dynamic nature of gene regulation: some relations are persistent across the full developmental cycle while many others are transient and specific to certain stages of development. For instance, five transcriptional factors, brk-pnt-zfh1-pros-dpp, form a long cascade of regulatory relations which are active across the full developmental cycle. Another example is gene Optix which are active across the full developmental cycle and serves as a hub for many other regulatory relations. As for transience of the regulatory relations, TFs to the right of Optix hub reduced in their activity as development proceeds to later stage. Furthermore, Optix connects two disjoint cascade of gene regulations to its left and right side after embryonic stage.

The dynamic networks also provide an overview of the interactions between genes from different functional groups. In Figure 13, we grouped genes according to 58 ontologies and visualized the connectivity between groups. We can see that large topological changes and network rewiring occur between functional groups. Besides expected interactions, the figure also reveals many seemingly unexpected interactions. For instance, during the transition from pupa stage to adult stage, *Drosophila* is undergoing a huge metamorphosis. One major feature of this metamorphosis is the development of the wing. As can be seen from Figure 13(r) and 13(s), genes related to metamorphosis, wing margin morphogenesis, wing vein morphogenesis and apposition of wing surfaces are among the most active group of genes, and they carry their activity into adult stage. Actually, many of these genes are also very active during early embryonic stage (for example, Figure 13(b) and 13(c)); the different is though they interact with different groups of genes. On one hand, the abundance of the transcripts from these genes at embryonic stage is likely due to maternal deposit (Arbeitman et al., 2002); on the other hand, this can also be due to the diverse functionalities of these genes. In Table 1, we listed 12 genes related to wing development of *Drosophila* which have a diverse number of other functions. We can see that many of these genes also play roles in normal cell growth, cell proliferation and embryonic development.

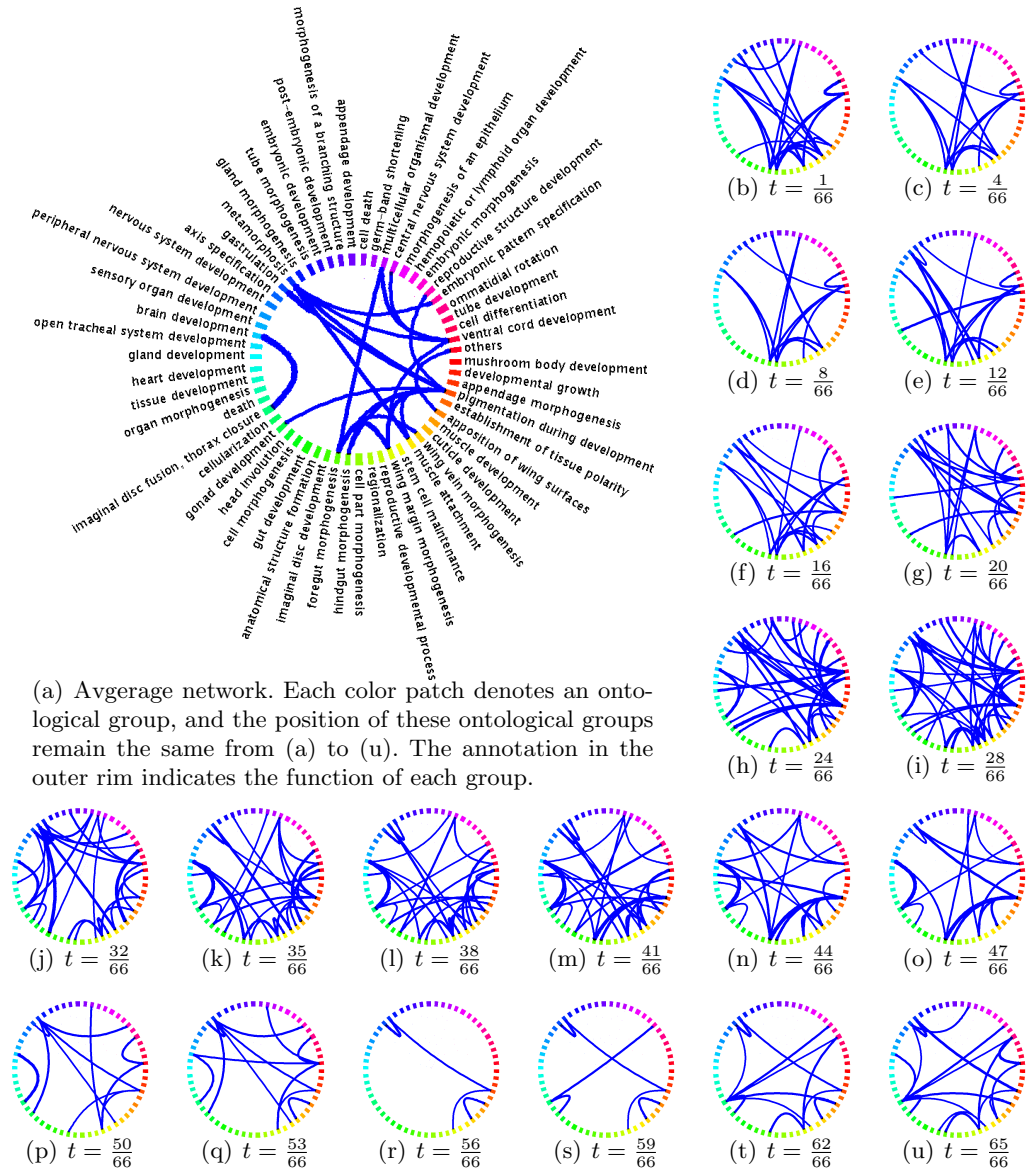


FIG 13. Interactions between gene ontological groups related to developmental process undergo dynamic rewiring. The weight of an edge between two ontological groups is the total number of connection between genes in the two groups. In the visualization, the width of an edge is proportional to its edge weight. We thresholded the edge weight at 30 in (b)-(u) so that only those interactions exceeding this number are displayed. The average network in (a) is produced by averaging the networks underlying (b)-(u). In this case, the threshold is set to 20 instead.

TABLE 1

Genes related to wing development also play roles in normal cell growth and embryonic development. Note that the genes in the left column of the table are all related to wing development. Hence in the right column of the table we only listed functions other than wing development.

Gene Name	Other Functions
dachs (d)	positive regulation of growth
moleskin (msk)	protein import into nucleus, docking, cell proliferation, compound eye development
extra macrochaetae (emc)	cell proliferation, nervous system development, sex determination
decapentaplegic (dpp)	anterior/posterior axis specification, cell fate specification, compound eye morphogenesis, heart development, germ-line stem cell division
Delta (Dl)	cell fate specification, compound eye development, mesoderm development, oogenesis, stem cell differentiation open tracheal system development,
schnurri (shn)	negative regulation of cell proliferation, midgut development, learning and/or memory
tolloid (tld)	embryonic pattern specification, terminal region determination, zygotic determination of dorsal/ventral axis, regulation of transforming growth factor
short stop (shot)	cell cycle arrest, muscle attachment, oocyte fate determination
rhea	cell adhesion, regulation of cell shape, muscle attachment, negative regulation of gene-specific transcription
held out wings (how)	cell differentiation, embryonic development, mesoderm development, somatic muscle development, regulation of alternative nuclear mRNA splicing
blistered (bs)	cell fate commitment, open tracheal system development
piopio (pio)	chitin-based embryonic cuticle biosynthetic process

5. Some properties of the algorithms. In this section we discuss some theoretical guarantees of the proposed algorithms. Mainly, we are interested in stating sufficient conditions under which the proposed methods are able to recover the unknown network correctly, i.e. they are model selection consistent. So far, we have managed to find conditions under which the kernel smoothing method is model selection consistent. These conditions are similar in nature to the conditions established in [Ravikumar et al. \(2008\)](#) where a neighborhood selection method was analysed in the context of static graphs.

The main result in this section concerns the scaling of the triple (n, p_n, s_n) under which the neighborhood selection procedure based on kernel smoothing is model selection consistent. The result we present is asymptotic in nature, however, we do not provide a classical asymptotic analysis where

one has fixed model and the sample size n is allowed to grow, instead, we consider the model dimension p_n and the maximum node degree s_n to be increasing functions of n . This approach gives more insight on the properties of the procedure, since it reflects the common situation arising in many applications where the number of features is larger than the sample size. As the model dimension to increase, we allow the estimation procedure to select a model that can represent a larger class of distribution.

The main quantity that will determine whether our algorithm will succeed or fail is the Hessian of the log-likelihood function evaluated at the true model parameter $\theta_{\setminus u}^{*,t}$. This quantity is a matrix $Q_u \in \mathbb{R}^{(p_n-1) \times (p_n-1)}$ defined for each node $u \in V$ as:

$$(14) \quad \begin{aligned} Q_u^{*,t} &:= \mathbb{E} \left[\nabla^2 \log \mathbb{P}_{\theta^{*,t}}[X_u | X_{\setminus u}] \right] \\ &= \mathbb{E} \left[\eta(X; \theta^{*,t}) X_{\setminus u} X_{\setminus u}^T \right], \end{aligned}$$

where $\eta(x; \theta) := \frac{4 \exp(2x_u \langle \theta_{\setminus u}, x_{\setminus u} \rangle)}{(\exp(2x_u \langle \theta_{\setminus u}, x_{\setminus u} \rangle) + 1)^2}$ is the variance function. This matrix is known as the Fisher information matrix and it plays a similar role in the covariance matrix $\mathbb{E}[X^t X^{tT}]$ of Gaussian graphical models in characterizing the success of the method. We will write Q^* for the matrix $Q_u^{*,t}$ and will assume that the conditions hold for every node $u \in V$. We will also drop explicit dependence on time when it is clear from context which time point we are referring to. We use $S = S_u^t := \{(u, v) | \theta_{uv}^t \neq 0\}$ as the index set of the edges that are in the neighborhood of the vertex u . S^c will denote its complement. Q_{SS}^* denotes the sub-matrix of Q^* indexed by S .

A1: Dependency condition The subset of the Fisher information matrix corresponding to the relevant features has bounded eigenvalues: there is a constant $C_{\min} > 0$ such that $\Lambda_{\min}(Q_{SS}^*) \geq C_{\min}$, $\forall t \in [0, 1]$. Furthermore, there is a constant $D_{\max} > 0$ such that $\Lambda_{\max}(\Sigma^*) \leq D_{\max}$, $\forall t \in [0, 1]$.

A2: Incoherence condition There is an incoherence parameter $\alpha \in (0, 1]$ such that $\|Q_{S^c S}^* (Q_{SS}^*)^{-1}\|_{\infty} \leq 1 - \alpha$, $\forall t \in [0, 1]$

A3: Smoothness conditions Let $\Sigma^{*,t} = [\sigma_{uv}(t)]$. There exist constants $A_0 > 0$, A such that $\max_{u,v} \sup_t |\sigma'_{uv}(t)| \leq A_0$ and $\max_{u,v} \sup_t |\sigma''_{uv}(t)| \leq A$. There also exists a constant $B_0 > 0$, B such that $\max_{u,v} \sup_t |\theta'_{uv}(t)| \leq B_0$ and $\max_{u,v} \sup_t |\theta''_{uv}(t)| \leq B$.

A4: The kernel function $K(\cdot)$ has a bounded support on $[-1, 1]$ and has the following properties

$$2 \int_{-1}^0 v K(v) dv \leq 2 \int_{-1}^0 K(v) dv = 1, \quad 2 \int_{-1}^0 v^2 K(v) dv \leq 1.$$

The conditions A1 and A2 guarantee that the procedure will be able to recover the true structure at each time point $t \in [0, 1]$. These conditions could be relaxed to hold only for points $t \in \mathcal{T}$. Note that these conditions are the same as for the i.i.d. case analyzed in [Ravikumar et al. \(2008\)](#), when the graph is stable over time, and they are related to conditions proposed in analysis of the linear regression (e.g. [Meinshausen and Bühlmann \(2006\)](#)). The condition A3 describes our notion of the distribution changing smoothly over time.

With these assumptions we are able to state our main result:

THEOREM 1. *Assume that A1, A2, A3 and A4 hold. Furthermore, assume that the following conditions hold:*

1. $h_n = \mathcal{O}(n^{-\frac{1}{3}})$
2. $s_n h_n = o(1)$, $\frac{s_n^3 \log p_n}{n h_n} = o(1)$ and $\lambda_1 = \mathcal{O}(\sqrt{\frac{\log p}{n h_n}})$
3. $\theta_{\min}^* = \Omega(\sqrt{\frac{s_n \log p_n}{n h_n}})$

Then for $t_0 \in [0, 1]$, the estimated graph $\hat{G}(\lambda_1, h_n, t_0)$ obtained through neighborhood selection satisfies

$$(15) \quad \mathbb{P} \left[\hat{G}(\lambda_1, h_n, t_0) \neq G^{t_0} \right] = \mathcal{O} \left(\exp \left(-C \frac{n h_n}{s_n^3} + C' \log p \right) \right) \rightarrow 0,$$

for some constants C, C' .

The theorem tells us that the procedure asymptotically recovers the graph, under appropriate regularization parameter λ_n as long as the ambient dimensionality p_n and the maximum node degree s_n are not too large, and minimum θ values do not tend to zero too fast.

Remarks:

1. The bandwidth parameter h_n is chosen so that it balances variance and squared bias of estimation of the elements of the Fisher information matrix.
2. Condition 2 requires that the size of the neighborhood of each node remains smaller than the size of the samples. However, the model ambient dimension p_n is allowed to grow exponentially in n .
3. Condition 3 is crucial to be able to distinguish true elements in the neighborhood of a node. We require that the size of the minimum element of the parameter vector stays bounded away from zero.

The proof of Theorem 1 is given in the appendix.

As of now, we do not have a characterization of the solution given by the algorithm TV. The main difficulty in obtaining a theoretical result for this procedure seems to be the analysis of the interaction between the ℓ_1 and $TV(\cdot)$ penalty.

The problem in equation (9) is related to the multiple change point detection in which one wants to find the "best" partition of $\{0, \frac{1}{n}, \dots, \frac{n-1}{n}, 1\}$ by intervals so that the unknown signal can be represented as a function of parameters that do not change over each interval. Usually one uses a penalty based on the number of intervals to select the "best" partition. The optimization based on this penalty function is intractable and one can use a TV penalty as an alternative. The relationship between use of a penalty based on a number of partitions and use of the TV penalty is similar to the relationship between the ℓ_0 penalty and the ℓ_1 penalty used in model selection for the classical linear regression.

Another relationship with model selection in the linear regression can be seen between the fussed lasso Tibshirani et al. (2005) and the TV penalty. As the TV penalty tries to select a partition of the space on which the features are defined, the fussed lasso tries to find a partition of the relevant features.

6. Discussion. We have presented an important problem of structure estimation of the time varying networks. While the structure estimation of the static networks is an important problem in itself, in certain cases the estimated static structure is of limited use. A static structure only shows connections and interactions that are persistent throughout the whole time period and more refined methods are needed to learn time varying structures. In this paper we have presented two methods that learn time varying networks from the observed discrete data. Even with these simple procedures, we are able to discover some patterns that would not be discovered using a method that estimates static networks. Being able to estimate more complex models comes with a price of more tuning parameters; the bandwidth parameter h_n and the penalty parameter λ_2 .

There are still many ways to improve the methods presented here. More principled ways of selecting tuning parameters are definitely needed. Selecting the tuning parameters in neighborhood selection procedure for static graphs is not an easy problem and estimating time varying graphs does not simplify the problem. Methods presented here do not allow for the incorporation of existing knowledge on the network topology into the algorithm. In some cases, data is very scarce and we would like to incorporate as much of the prior knowledge into the procedure, so directing research towards finding Bayesian flavored algorithms seems very important.

Two methods presented here present two different ends of the spectrum: one algorithm is able to estimate smoothly changing networks, while the other is more tailored towards estimation of structural changes in the model. It is important to combine the two. There is a great amount of work in nonparametric estimation of change points and it would be interesting to try to make use of some of those methods for estimating time varying networks.

Appendix. In this appendix we very briefly outline the main proof idea of Theorem 1. The proof itself is quite technical and we plan to present it in a separate publication. The main idea is that when the assumptions A1 to A4 are satisfied, for appropriately chosen tuning parameters h_n and λ_1 , the empirical estimate \hat{Q} of the Fisher information matrix Q^* will, with high probability, satisfy A1 and A2. Conditioned on the event that the estimate \hat{Q} has these "good properties" A1 and A2, the structure of the network will be estimated correctly, also with high probability. This line of reasoning is not new and was employed in Ravikumar et al. (2008) to prove model selection consistency of the neighborhood selection method for static networks. The time varying networks present a lot of technical issues, however.

We outline the proof of Theorem 1 for a fixed time point t_0 . Let us define a "good" event \mathcal{E} , on which we can show that the probability of estimating a wrong neighborhood of node u is converging to 0, i.e. $\mathbb{P}[\widehat{\mathcal{N}}(u, t_0) \neq \mathcal{N}(u, t_0) | \mathcal{E}] \rightarrow 0$. Under the assumptions A1 to A4, it can be shown that the event \mathcal{E} happens with probability converging to 1, i.e. $\mathbb{P}[\mathcal{E}^c] \rightarrow 0$. From these two parts, we obtain that the neighborhood estimation of each node can be achieved exponentially fast, and the main result follows from applying the union bound over all p_n nodes.

Let $\hat{Q} \equiv \hat{Q}_u = \sum_t w_t \eta(x^t; \theta^{*, t_0}) x_{\setminus u}^t x_{\setminus u}^{tT}$ denote the estimate of the Fisher information matrix and let $\hat{\Sigma} \equiv \hat{\Sigma}_u = \sum_t w_t x_{\setminus u}^t x_{\setminus u}^{tT}$ denote the estimate of the covariance matrix at time point t_0 . The "good" event is defined as

$$(16) \quad \mathcal{E} = \{ \mathcal{D}_n \mid \hat{Q} \text{ and } \hat{\Sigma} \text{ satisfy assumptions A1 and A2 } \}.$$

The two main technical difficulties that we have to deal with are: (1) we have to show that the estimate \hat{Q} converges to Q^* for matrices of increasing size and (2) we do not have the i.i.d. sample, so we cannot use standard large deviation bounds.

On the event \mathcal{E} , we can show that the neighborhood selection procedure selects the model consistently analyzing the Karush-Kuhn-Tucker (KKT) conditions associated with the convex problem (4). A constructive procedure can be given that produces a solution that satisfies the KKT conditions with high probability. We have the following result:

LEMMA 2. *Assume that the assumptions A1 and A2 hold for the estimate \hat{Q} . If the following conditions hold*

1. $h_n = \mathcal{O}(n^{-\frac{1}{3}})$
2. $s_n h_n = o(1)$, $\frac{s_n^2 \log p}{nh_n} = o(1)$ and $\lambda_n = \mathcal{O}(\sqrt{\frac{\log p}{nh_n}})$
3. $\theta_{\min}^* = \Omega(\sqrt{\frac{s_n \log p_n}{nh_n}})$,

then for $t_0 \in [0, 1]$, the estimated graph $\hat{G}(\lambda_n, t_0)$ obtained through neighborhood selection satisfies

$$(17) \quad \mathbb{P}[\hat{G}(\lambda_n, t_0) = G^{t_0} \mid \mathcal{E}] = \mathcal{O}(\exp(-Cnh_n\lambda_n^2 + C' \log p))$$

for some constants C, C' .

The remainder of the argument goes by showing that the event \mathcal{E} happens with high probability. To show this, we bound the deviation between elements of $\hat{Q} = [\hat{q}_{uv}(t_0)]$ and $Q^{*,t_0} = [q_{uv}(t_0)]$. We use the following decomposition

$$(18) \quad \begin{aligned} |\hat{q}_{uv}(t_0) - q_{uv}(t_0)| &\leq \left| \sum_t w_t \eta(x^t; \theta^{*,t_0}) x_u^t x_v^t - \sum_t w_t \eta(x^t; \theta^{*,t}) x_u^t x_v^t \right| \\ &+ \left| \sum_t w_t \eta(x^t; \theta^{*,t}) x_u^t x_v^t - \mathbb{E}[\sum_t w_t \eta(x^t; \theta^{*,t}) x_u^t x_v^t] \right| \\ &+ \left| \mathbb{E}[\sum_t w_t \eta(x^t; \theta^{*,t}) x_u^t x_v^t] - q_{uv}(t_0) \right| \end{aligned}$$

and proceed with bounding each individual term. The following lemma gives us behaviour of the terms in (18).

LEMMA 3. *Assume that the conditions of Theorem 1 and A3 are satisfied. Let $Z_{uv}^t = w_t \eta(X^t; \theta^{*,t}) X_u^t X_v^t$. There is a constant $C > 0$, depending on $K(\cdot)$ only, such that for any $t_0 \in [0, 1]$:*

$$(19) \quad \max_{u,v} |\hat{q}_{uv}(t_0) - \sum_t w_t \eta(x^t; \theta^{*,t}) x_u^t x_v^t| = \mathcal{O}(s_n h_n)$$

$$(20) \quad \mathbb{P}[|\sum_t (Z_{uv}^t - \mathbb{E}[Z_{uv}^t])| > \epsilon] \leq 2 \exp(-Cnh_n \epsilon^2)$$

$$(21) \quad \max_{u,v} |\mathbb{E}[\sum_t w_t \eta(x^t; \theta^{*,t}) x_u^t x_v^t] - q_{uv}(t_0)| = \mathcal{O}(h_n).$$

Now, we are ready to state the results that show that the estimate \hat{Q} satisfies A1 and A2:

LEMMA 4. Under assumptions A1 and A3 and any $t_0 \in [0, 1]$, we have

$$(22) \quad \Lambda_{\min}(\hat{Q}_{SS}) \geq C_{\min} - \mathcal{O}_p\left(\sqrt{\frac{s_n^2 \log s_n}{nh_n}} + s_n h_n\right).$$

LEMMA 5. Under assumptions A2, A3, for any $t_0 \in [0, 1]$, we have

$$(23) \quad \|\hat{Q}_{S^c S}(\hat{Q}_{SS})^{-1}\|_{\infty} \leq 1 - \frac{\alpha}{2}$$

with probability $1 - \mathcal{O}(\exp(-C\frac{nh_n}{s_n^3} + C' \log p))$.

Similarly we can show that the estimate $\hat{\Sigma}$ satisfies the assumption A1. We omit the details.

Putting Lemmas 2, 3, 4, 5 together we prove Theorem 1.

References.

- M. Arbeitman, E. Furlong, F. Imam, E. Johnson, B. Null, B. Baker, M. Krasnow, M. Scott, R. Davis, and K. White. Gene expression during the life cycle of *Drosophila melanogaster*. *Science*, 297:2270–2275, 2002.
- O. Banerjee, L. El Ghaoui, and A. d’Aspremont. Model selection through sparse maximum likelihood estimation. *J. Mach. Learn. Res.*, 9:485–516, 2008.
- E. H. Davidson. *Genomic Regulatory Systems*. Academic Press, 2001.
- P. L. Davies and A. Kovac. Local extremes, runs, strings and multiresolution. *The Annals of Statistics*, 29(1):1–48, 2001. ISSN 00905364.
- M. Drton and M. D. Perlman. Model selection for Gaussian concentration graphs. *Biometrika*, 91(3):591–602, 2004. .
- J. Duchi, S. Gould, and D. Koller. Projected subgradient methods for learning sparse gaussians. In *Proceedings of the Twenty-fourth Conference on Uncertainty in AI (UAI)*, 2008a.
- J. Duchi, S. S. Shwartz, Y. Singer, and T. Chandra. Efficient projections onto the l1-ball for learning in high dimensions. In *ICML ’08: Proceedings of the 25th international conference on Machine learning*, pages 272–279, New York, NY, USA, 2008b. ACM. ISBN 978-1-60558-205-4.
- B. Efron, T. Hastie, I. Johnstone, and R. Tibshirani. Least angle regression. *Annals of Statistics*, 32(2):407–499, 2004.
- J. Fan and R. Li. Variable selection via nonconcave penalized likelihood and its oracle properties. *Journal of the American Statistical Association*, 96:1348–1360, December 2001.
- J. Fan, Y. Feng, and Y. Wu. Network exploration via the adaptive lasso and scad penalties. *Annals of Applied Statistics*, to appear, December 2008.
- J. Friedman, T. Hastie, H. Hofling, and R. Tibshirani. Pathwise coordinate optimization. *ANNALS OF APPLIED STATISTICS*, 1:302, 2007a. .
- J. Friedman, T. Hastie, and R. Tibshirani. Sparse inverse covariance estimation with the graphical lasso. *Biostat*, page kxm045, 2007b. .
- J. Friedman, T. Hastie, and R. Tibshirani. Regularization paths for generalized linear models via coordinate descent, 2008.

- M. Grant and S. Boyd. Cvx: Matlab software for disciplined convex programming (web page and software), 2008. URL <http://stanford.edu/~boyd/cvx>.
- F. Guo, S. Hanneke, W. Fu, and E. P. Xing. Recovering temporally rewiring networks: A model-based approach. *International Conference of Machine Learning*, 2007.
- S. Hanneke and E.P Xing. Discrete temporal models of social networks. *Workshop on Statistical Network Analysis, the 23rd International Conference on Machine Learning (ICML-SNA)*, 2006.
- K. Koh, S.-J. Kim, and S. Boyd. An interior-point method for large-scale ℓ_1 -regularized logistic regression. *J. Mach. Learn. Res.*, 8:1519–1555, 2007. ISSN 1533-7928.
- S. L. Lauritzen. *Graphical Models (Oxford Statistical Science Series)*. Oxford University Press, USA, July 1996.
- N. Luscombe, M. Babu, H. Yu, M. Snyder, S. Teichmann, and M. Gerstein. Genomic analysis of regulatory network dynamics reveals large topological changes. *Nature*, 431:308–312, 2004.
- E. Mammen and S. van de Geer. Locally adaptive regression splines. *The Annals of Statistics*, 25(1):387–413, 1997. ISSN 00905364.
- N. Meinshausen and P. Bühlmann. High-dimensional graphs and variable selection with the lasso. *Annals of Statistics*, 34:1436, 2006.
- J. Peng, P. Wang, N. Zhou, and J. Zhu. Partial correlation estimation by joint sparse regression models. 2008.
- P. Ravikumar, M. J. Wainwright, G. Raskutti, and B. Yu. High-dimensional covariance estimation by minimizing ℓ_1 -penalized log-determinant divergence. Nov 2008.
- A. J. Rothman, P. J. Bickel, E. Levina, and J. Zhu. Sparse permutation invariant covariance estimation. *ELECTRONIC JOURNAL OF STATISTICS*, 2:494, 2008.
- L. I. Rudin, S. Osher, and E. Fatemi. Nonlinear total variation based noise removal algorithms. *Phys. D*, 60(1-4):259–268, 1992. ISSN 0167-2789. .
- P. Sarkar and A. Moore. Dynamic social network analysis using latent space models. *Conference of Knowledge Discovery and Data Mining*, 2006.
- R. Tibshirani, M. Saunders, S. Rosset, J. Zhu, and K. Knight. Sparsity and smoothness via the fused lasso. *Journal Of The Royal Statistical Society Series B*, 67(1):91–108, 2005.
- P. Tseng. Convergence of a block coordinate descent method for nondifferentiable minimization. *J. Optim. Theory Appl.*, 109(3):475–494, 2001. ISSN 0022-3239.
- M. J. Wainwright. Sharp thresholds for high-dimensional and noisy recovery of sparsity, 2006.
- M. J. Wainwright, P. Ravikumar, and J. D. Lafferty. High-dimensional graphical model selection using ℓ_1 -regularized logistic regression. In Bernhard Schölkopf, John Platt, and Thomas Hoffman, editors, *NIPS*, pages 1465–1472. MIT Press, 2006. ISBN 0-262-19568-2.
- D. Watts and S. Strogatz. Collective dynamics of ‘small-world’ networks. *Nature*, 393(6684):440–442, 1998.
- M. Yuan and Y. Lin. Model election and estimation in the Gaussian graphical model. *Biometrika*, page asm018, 2007. .
- P. Zhao and B. Yu. On model selection consistency of lasso. *J. Mach. Learn. Res.*, 7:2541–2563, 2006. ISSN 1533-7928.
- S. Zhou, J. Lafferty, and L. Wasserman. Time varying undirected graphs. In Rocco A. Servedio and Tong Zhang, editors, *COLT*, pages 455–466. Omnipress, 2008.
- H. Zou and R. Li. One-step sparse estimates in nonconcave penalized likelihood models. *ANNALS OF STATISTICS*, 36:1509, 2008.

ADDRESS OF THE AUTHORS
5000 FORBES AVE, WEAN HALL 4212
PITTSBURGH, PA 15213
E-MAIL: mladenk@cs.cmu.edu
lesong@cs.cmu.edu
amahmed@cs.cmu.edu
epxing@cs.cmu.edu